

Do physics-informed neural networks (PINNs) need to be deep? Shallow PINNs using the Levenberg–Marquardt algorithm

Muhammad Luthfi Shahab^{a,b}, Imam Mukhlash^a, Hadi Susanto^{b,c}

^a*Department of Mathematics, Institut Teknologi Sepuluh Nopember, Surabaya, 60111, Indonesia*

^b*Department of Mathematics, Khalifa University of Science & Technology, Abu Dhabi, PO Box 127788, United Arab Emirates*

^c*Department of Mathematics, Faculty of Mathematics and Natural Sciences, Universitas Indonesia, Gedung D Lt. 2 FMIPA Kampus UI, Depok, 16424, Indonesia*

Abstract

This work investigates the use of shallow physics-informed neural networks (PINNs) for solving forward and inverse problems of nonlinear partial differential equations (PDEs). By reformulating PINNs as nonlinear systems, the Levenberg–Marquardt (LM) algorithm is employed to efficiently optimize the network parameters. Analytical expressions for the neural network derivatives with respect to the input variables are derived, enabling accurate and efficient computation of the Jacobian matrix required by LM. The proposed approach is tested on several benchmark problems, including the Burgers, Schrödinger, Allen–Cahn, and three-dimensional Bratu equations. Numerical results demonstrate that LM significantly outperforms BFGS in terms of convergence speed, accuracy, and final loss values, even when using shallow network architectures with only two hidden layers. These findings indicate that, for a wide class of PDEs, shallow PINNs combined with efficient second-order optimization methods can provide accurate and computationally efficient solutions for both forward and inverse problems.

Keywords: Physics-informed neural networks (PINNs), Shallow neural networks, Nonlinear systems, Levenberg–Marquardt algorithm, Forward and inverse PDEs

1. Introduction

In recent years, a variety of deep learning-based approaches have been proposed for the numerical solution of partial differential equations (PDEs). Representative examples include physics-informed neural networks (PINNs)

[1], deep learning methods for high-dimensional PDEs [2, 3], deep operator networks (DeepONet) [4], and Fourier neural operators (FNOs) [5]. Among these approaches, PINNs have attracted particular attention due to their flexibility and their ability to incorporate governing equations directly into the learning process.

Although the PINNs framework was popularized by Raissi et al. [1], related ideas had been explored earlier, especially for forward problems. Early contributions include the works of Lee and Kang [6], Dissanayake and Phan-Thien [7], and Lagaris et al. [8, 9]. Raissi et al. [1] significantly extended these ideas by addressing both forward and inverse problems for time-dependent PDEs using deep neural networks. In the PINNs framework, the governing PDEs and available data are incorporated into a composite loss function, which is typically minimized using first-order optimizers such as Adam [10] or quasi-Newton methods such as LBFGS [11]. Recent studies have shown that BFGS, self-scaled BFGS (SSBFGS), and self-scaled Broyden (SSBroyden) methods can outperform LBFGS in terms of solution accuracy for PINNs [12], thereby motivating renewed interest in second-order optimization techniques.

Early PINN studies predominantly employed deep neural networks. However, deep architectures often incur high computational cost and training inefficiencies [13]. To mitigate these issues, several alternatives based on shallow or parsimonious neural architectures have been proposed. These include shallow neural networks [14], extreme learning machines (ELMs) [15], and random projection-based neural networks [16]. For example, Schiassi et al. [17] introduced the extreme theory of functional connections (X-TFC), which employs a single-layer neural network trained via ELM. Dwivedi and Srinivasan [18] proposed physics-informed extreme learning machines for linear PDEs, while Ramabathiran and Ramachandran [19] developed sparse and partially interpretable PINNs (SPINNs) for ODEs and PDEs. Hu et al. [14] constructed shallow PINNs for PDEs defined on static and evolving surfaces. Additional related developments can be found in [20, 21, 22, 23, 16].

Motivated by these developments, this work focuses on shallow PINNs and formulates their training process as the solution of nonlinear systems or nonlinear least-squares problems. This perspective naturally enables the use of the Levenberg–Marquardt (LM) algorithm [24, 25], a classical second-order method designed for such problems. LM has been extensively studied in the neural network literature. Early work by Hagan and Menhaj [26] demonstrated its effectiveness for training feed-forward neural networks with a moderate number of parameters. Subsequent improvements addressing memory usage and computational efficiency were proposed in [27, 28], and LM has been successfully applied in various engineering and control applica-

tions [29, 30].

Within the context of PINNs, the application of LM has so far been mainly restricted to time-independent problems. Calandra et al. [31] developed a multilevel LM strategy for stationary PDEs, while Yadav and Srinivasan [32] applied LM to singular perturbation problems. More recently, Shahab et al. [33, 34, 35] reformulated PINNs as nonlinear systems and employed LM to compute steady-state solutions and bifurcation diagrams, demonstrating that shallow neural networks with only a few hundred parameters can accurately capture nonlinear dynamics. In contrast, applications of LM to time-dependent PDEs within the PINNs framework remain relatively limited. One notable example is the work of Taylor et al. [36], who applied LM to a regression task and to a single forward problem involving the Burgers equation.

The objective of this work is to extend the application of LM within the PINNs framework to both time-dependent and time-independent PDEs, addressing forward and inverse problems. A further objective is to examine whether deep neural networks are essential for achieving high accuracy in PINNs, or whether shallow architectures combined with effective second-order optimization methods can provide comparable performance.

To assess the proposed approach, numerical experiments are conducted on four nonlinear PDEs in both forward and inverse problems, including the Burgers, Schrödinger, Allen–Cahn [1], and three-dimensional Bratu equations [37]. The performance of LM is compared with that of BFGS, as well as with representative results reported in the original PINNs literature. In addition, exact analytical expressions for neural network derivatives are derived, the architecture of PINNs is presented to clarify the sharing of weights and biases between the solution and its derivatives, and explicit Jacobian formulations for LM iterations are provided. The relationship between these Jacobian-based formulations and gradient computations used in standard optimization methods is also discussed.

The remainder of this paper is organized as follows. Section 2 presents the formulation of PINNs as nonlinear systems and describes the application of LM to forward and inverse problems. Section 3 reports numerical results and performance comparisons. Section 4 concludes the paper and outlines directions for future research.

2. Proposed PINNs

In this section, we describe the proposed PINNs framework for both forward and inverse problems and highlight its connections to and differences from the standard PINNs approach.

Table 1: Dimensions of the weight matrices and bias vectors for the network $\text{NN}(a, m_1, m_2, 1)$.

Name	Size	Description
W_1	$a \times m_1$	Weights between the input and first hidden layers
B_1	$1 \times m_1$	Biases between the input and first hidden layers
W_2	$m_1 \times m_2$	Weights between the first and second hidden layers
B_2	$1 \times m_2$	Biases between the first and second hidden layers
W_3	$m_2 \times 1$	Weights between the second hidden and output layers
B_3	1×1	Bias between the second hidden and output layers

2.1. Shallow neural networks

We first describe the neural network architecture employed in this work. Specifically, we consider shallow feed-forward neural networks with two hidden layers. In such architectures, the largest number of trainable parameters typically arises from the connections between the two hidden layers.

Throughout this paper, the notation $\text{NN}(a, m_1, m_2, 1)$ denotes a neural network with a inputs, m_1 neurons in the first hidden layer, m_2 neurons in the second hidden layer, and a single output. Let $W = \{W_1, B_1, W_2, B_2, W_3, B_3\}$ denote the set of all weights and biases. For time-dependent PDEs with one spatial variable, the neural network output $\tilde{u}(x, t, W)$ is defined as

$$\tilde{u}(x, t, W) = \sigma(\sigma([x \ t]W_1 + B_1)W_2 + B_2)W_3 + B_3, \quad (1)$$

where $\sigma(\cdot)$ is a nonlinear activation function and $[x \ t]$ is a row vector containing the spatial and temporal input variables. The dimensions of the weights and biases are summarized in Tab. 1. For problems with additional spatial variables or without a temporal variable, only the dimension of W_1 needs to be adjusted accordingly.

When neural networks are used to approximate solutions of PDEs, it is often advantageous to enforce the initial and boundary conditions directly within the network representation. This can be achieved by modifying the neural network output as

$$u(x, t, W) = \tilde{u}(x, t, W) \cdot p(x, t) + q(x), \quad (2)$$

where the functions $p(x, t)$ and $q(x)$ are constructed such that $u(x, t, W)$ satisfies the prescribed initial and boundary conditions.

Throughout the remainder of this paper, initial and boundary conditions are enforced using this approach. This strategy typically improves training efficiency and solution accuracy [38]. For clarity, \tilde{u} and u are used to denote the neural network output before and after enforcing the initial and boundary conditions, respectively.

2.2. PINNs for the forward problem

Consider a general PDE of the form

$$u_t + \mathcal{N}(u) = 0, \quad x \in \Omega, \quad t \in [0, T], \quad (3)$$

with certain initial and boundary conditions, where $\mathcal{N}(\cdot)$ denotes a nonlinear differential operator. In the forward problem setting, given the complete form of the governing PDE, the objective is to approximate the solution $u(x, t)$ over the spatiotemporal domain.

We approximate the solution by a neural network $u(x, t, W)$, where W denotes the collection of all weights and biases. Let $\{(x_i, t_i)\}_{i=1}^n$ be a set of n collocation points sampled from the domain. Assuming that the initial and boundary conditions are enforced through the network construction [38], the network parameters are determined by minimizing the loss function

$$L(W) = \frac{1}{n} \sum_{i=1}^n (f_i(W))^2, \quad (4)$$

where

$$f_i(W) = u_t(x_i, t_i, W) + \mathcal{N}(u(x_i, t_i, W)), \quad i = 1, \dots, n, \quad (5)$$

represents the residual of the PDE.

In the original PINNs framework, this minimization problem is typically solved using the limited-memory BFGS (LBFGS) algorithm [11]. However, a more recent study has shown that BFGS may offer improved performance in training PINNs [12]. In standard implementations, the spatial and temporal derivatives of $u(x, t, W)$, as well as the gradients of the loss function with respect to the network parameters, are computed using automatic differentiation [39].

In contrast, we propose a different formulation in this work. Rather than minimizing the loss function (4), we reformulate the problem as solving a nonlinear system of equations, or equivalently a nonlinear least-squares problem, of the form

$$F(W) = \begin{bmatrix} f_1(W) \\ \vdots \\ f_n(W) \end{bmatrix} = \mathbf{0}, \quad (6)$$

where $f_i(W)$ is defined as in Eq. (5). This system is solved using the Levenberg–Marquardt (LM) algorithm [24, 25], a robust and efficient optimization method that blends the Gauss–Newton algorithm and gradient descent, making it well-suited for least-squares problems.

The implementation of LM requires the Jacobian matrix J of $F(W)$ at each iteration, consisting of the partial derivatives of each residual $f_i(W)$ with respect to all network parameters in W . To evaluate these residuals, the derivatives of $u(x, t, W)$ with respect to x and t must first be computed.

Although such derivatives can be obtained using automatic differentiation available in deep learning libraries such as TensorFlow [40], it is important to note that support for LM is not readily available in modern frameworks. Therefore, in this work, we develop an exact analytical differentiation scheme for computing the required Jacobian matrix. This approach enables the effective application of LM to PINNs and, at the same time, provides additional insight into the internal structure and optimization dynamics of PINNs.

2.2.1. Derivatives with respect to x and t

In this subsection, we present an analytical procedure for computing the derivatives of the neural network functions \tilde{u} and u with respect to the input variables x and t . We begin with the neural network output \tilde{u} defined in Eq. (1). For clarity and ease of differentiation, the network operations are rewritten in a layer-wise form:

$$\begin{aligned} X &= [x \ t], \\ h_1 &= XW_1 + B_1, \\ H_1 &= \sigma(h_1), \\ h_2 &= H_1W_2 + B_2, \\ H_2 &= \sigma(h_2), \\ \tilde{u} &= H_2W_3 + B_3. \end{aligned} \tag{7}$$

Here, h_ℓ and H_ℓ denote the pre-activation and post-activation variables of the ℓ -th hidden layer, respectively, and $\sigma(\cdot)$ is a nonlinear activation function, such as the hyperbolic tangent.

We first compute the partial derivative of \tilde{u} with respect to t . Since $X = [x \ t]$, its derivative with respect to t is given by $X_t = [0 \ 1]$, which leads to

$$\begin{aligned} X_t &= [0 \ 1], \\ h_{1,t} &= X_t W_1, \\ H_{1,t} &= \sigma'(h_1) \cdot h_{1,t}, \\ h_{2,t} &= H_{1,t} W_2, \\ H_{2,t} &= \sigma'(h_2) \cdot h_{2,t}, \\ \tilde{u}_t &= H_{2,t} W_3. \end{aligned} \tag{8}$$

Similarly, the derivative of \tilde{u} with respect to x is obtained using $X_x = [1 \ 0]$:

$$\begin{aligned} X_x &= [1 \ 0], \\ h_{1,x} &= X_x W_1, \\ H_{1,x} &= \sigma'(h_1) \cdot h_{1,x}, \\ h_{2,x} &= H_{1,x} W_2, \\ H_{2,x} &= \sigma'(h_2) \cdot h_{2,x}, \\ \tilde{u}_x &= H_{2,x} W_3. \end{aligned} \tag{9}$$

Proceeding further, the second derivative of \tilde{u} with respect to x is given by

$$\begin{aligned} X_{xx} &= [0 \ 0], \\ h_{1,xx} &= X_{xx} W_1, \\ H_{1,xx} &= \sigma''(h_1) \cdot h_{1,x}^2 + \sigma'(h_1) \cdot h_{1,xx}, \\ h_{2,xx} &= H_{1,xx} W_2, \\ H_{2,xx} &= \sigma''(h_2) \cdot h_{2,x}^2 + \sigma'(h_2) \cdot h_{2,xx}, \\ \tilde{u}_{xx} &= H_{2,xx} W_3. \end{aligned} \tag{10}$$

Although X_{xx} and $h_{1,xx}$ vanish in the present setting, we retain this formulation for generality. In many applications, the input variables may undergo nonlinear transformations (e.g., $\sin(x)$ or $\cos(x)$) prior to being fed into the network, which results in nonzero second derivatives. The above structure therefore remains applicable to a broader class of problems.

When initial and boundary conditions are enforced through the transformation introduced in Eq. (2), the final approximations of u and its derivatives are given by

$$\begin{aligned} u &= \tilde{u} \cdot p(x, t) + q(x), \\ u_t &= \tilde{u}_t \cdot p(x, t) + \tilde{u} \cdot p_t(x, t), \\ u_x &= \tilde{u}_x \cdot p(x, t) + \tilde{u} \cdot p_x(x, t) + q_x(x), \\ u_{xx} &= \tilde{u}_{xx} \cdot p(x, t) + 2\tilde{u}_x \cdot p_x(x, t) + \tilde{u} \cdot p_{xx}(x, t) + q_{xx}(x). \end{aligned} \tag{11}$$

For simplicity, only derivatives up to second order in x are presented; higher-order derivatives can be derived analogously. The procedure also extends straightforwardly to deeper network architectures. Once we compute u , u_t , u_x , and u_{xx} , we can plug these into the nonlinear system $F(W)$ defined in Eq. (6) to proceed with training.

All computations above naturally extend to a vectorized setting. Let \mathbf{x} and \mathbf{t} denote vectors corresponding to n collocation points. Then,

$$X = [\mathbf{x} \ \mathbf{t}], \quad X_t = [\mathbf{0} \ \mathbf{1}], \quad X_x = [\mathbf{1} \ \mathbf{0}], \quad X_{xx} = [\mathbf{0} \ \mathbf{0}], \tag{12}$$

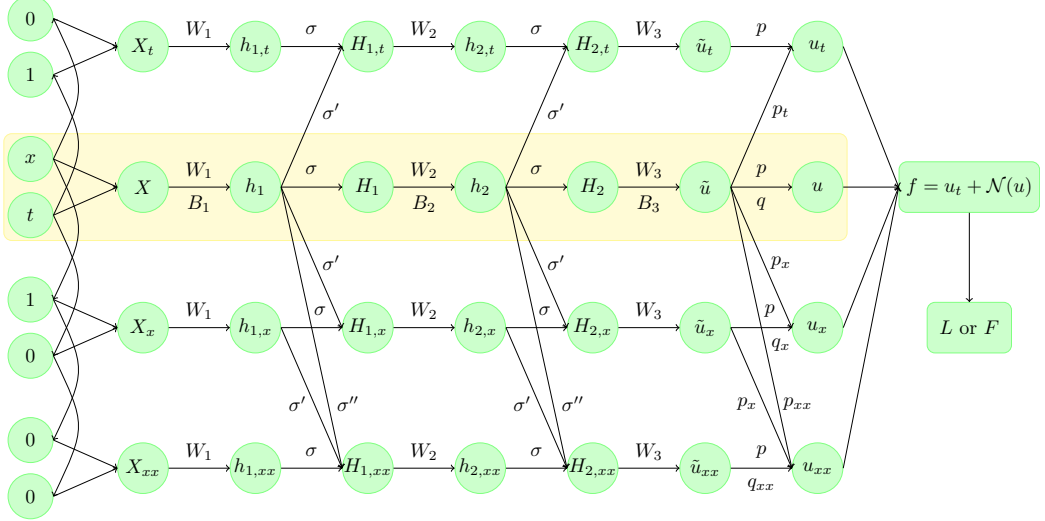


Figure 1: Explicit representation of the internal PINN architecture, illustrating how the core network \tilde{u} (yellow) and its spatial and temporal derivatives are analytically constructed from shared weights and biases.

where **0** and **1** are vectors of zeros and ones of appropriate dimensions.

For a network with architecture $\text{NN}(2, m_1, m_2, 1)$, the matrices h_1 and H_1 have dimensions $n \times m_1$, while h_2 and H_2 are of size $n \times m_2$. In the vectorized formulation, the dot operator \cdot in Eqs. (8)–(11) denotes element-wise multiplication, whereas products such as XW_1 correspond to standard matrix multiplication.

Fig. 1 illustrates the overall structure of PINNs and the relationships between \tilde{u} and its derivatives \tilde{u}_t , \tilde{u}_x , and \tilde{u}_{xx} . The yellow block represents the main forward pass computing \tilde{u} , while the derivative computations reuse the same weights W_1 , W_2 , and W_3 , as well as intermediate quantities such as h_1 and h_2 . The derivatives are independent of the final bias B_3 , which only affects \tilde{u} . After enforcing the initial and boundary conditions, however, all weights and biases contribute to the final approximation u and its derivatives.

To compute higher-order derivatives of u , higher-order derivatives of the activation function σ and of the auxiliary functions $p(x, t)$ and $q(x)$ are required. Finally, although each hidden layer consists of multiple neurons, it is represented by a single node in Fig. 1 for clarity, allowing the figure to emphasize data flow and dependency structure rather than architectural details.

To the best of our knowledge, such an explicit and complete illustration of the internal architecture of PINNs and its analytical connections to spatial and temporal derivatives has not been presented in previous studies.

Most existing works rely on automatic differentiation to compute derivatives, which obscures the precise dependency structure between the neural network parameters and the resulting differential operators. By deriving and visualizing these relationships explicitly, our framework provides new insight into the internal mechanics of PINNs and clarifies how solution values and their derivatives are jointly constructed from shared network parameters.

2.2.2. Jacobian

As discussed earlier, since PINNs are reformulated here as nonlinear systems and optimized using LM, the computation of the Jacobian matrix is a key component at each iteration.

To this end, all weights and biases of the neural network, namely W_1, B_1, W_2, B_2, W_3 , and B_3 , are first reshaped into row vectors and concatenated into a single column vector

$$W = [W_1 \ B_1 \ W_2 \ B_2 \ W_3 \ B_3]^T. \quad (13)$$

Let m denote the total number of trainable parameters, so that $W \in \mathbb{R}^m$. Given a set of n collocation points, $\{(x_i, t_i)\}_{i=1}^n$, the Jacobian matrix $J \in \mathbb{R}^{n \times m}$ is defined by

$$J = \begin{bmatrix} \frac{\partial f_1}{\partial w_1} & \dots & \frac{\partial f_1}{\partial w_m} \\ \vdots & \ddots & \vdots \\ \frac{\partial f_n}{\partial w_1} & \dots & \frac{\partial f_n}{\partial w_m} \end{bmatrix}, \quad (14)$$

where w_r , $r = 1, \dots, m$, denotes the r -th component of W .

The (i, r) -th entry of the Jacobian matrix is given by

$$\begin{aligned} J_{i,r} &= \frac{\partial f_i}{\partial w_r} \\ &= \frac{\partial(u_t(x_i, t_i, W) + \mathcal{N}(u(x_i, t_i, W)))}{\partial w_r} \\ &= \frac{\partial u_t(x_i, t_i, W)}{\partial w_r} + \mathcal{N}_{w_r}(u(x_i, t_i, W)), \end{aligned} \quad (15)$$

where $\mathcal{N}_{w_r}(\cdot)$ denotes the partial derivative of the nonlinear operator \mathcal{N} with respect to w_r , which generally involves derivatives of u , u_x , and u_{xx} with respect to w_r .

As an illustrative example, consider the nonlinear operator

$$\mathcal{N}(u) = uu_x - \frac{0.01}{\pi}u_{xx}. \quad (16)$$

Its derivative with respect to w_r is then given by

$$\mathcal{N}_{w_r}(u) = \frac{\partial u}{\partial w_r} u_x + u \frac{\partial u_x}{\partial w_r} - \frac{0.01}{\pi} \frac{\partial u_{xx}}{\partial w_r}. \quad (17)$$

Consequently, the construction of the Jacobian matrix requires closed-form expressions for $\frac{\partial u}{\partial w_r}$, $\frac{\partial u_t}{\partial w_r}$, $\frac{\partial u_x}{\partial w_r}$, and $\frac{\partial u_{xx}}{\partial w_r}$.

It is worth noting that these derivatives depend strongly on the position of w_r within the network architecture. Parameters located closer to the output layer lead to simpler derivative expressions, while parameters near the input layer involve increasingly complex chain-rule expansions. This observation highlights an important computational advantage of shallow architectures: for a fixed number of parameters, shallower networks generally yield lower Jacobian evaluation costs. In [Appendix A](#), we provide all explicit formulas for computing the derivatives of \tilde{u} , \tilde{u}_t , \tilde{u}_x , and \tilde{u}_{xx} with respect to w_r , depending on its location in the network.

Additionally, since the initial and boundary conditions are enforced using Eq. (11), the corresponding derivatives of u and its temporal and spatial derivatives are given by

$$\begin{aligned} \frac{\partial u}{\partial w_r} &= \frac{\partial \tilde{u}}{\partial w_r} \cdot p(x, t), \\ \frac{\partial u_t}{\partial w_r} &= \frac{\partial \tilde{u}_t}{\partial w_r} \cdot p(x, t) + \frac{\partial \tilde{u}}{\partial w_r} \cdot p_t(x, t), \\ \frac{\partial u_x}{\partial w_r} &= \frac{\partial \tilde{u}_x}{\partial w_r} \cdot p(x, t) + \frac{\partial \tilde{u}}{\partial w_r} \cdot p_x(x, t), \\ \frac{\partial u_{xx}}{\partial w_r} &= \frac{\partial \tilde{u}_{xx}}{\partial w_r} \cdot p(x, t) + 2 \frac{\partial \tilde{u}_x}{\partial w_r} \cdot p_x(x, t) + \frac{\partial \tilde{u}}{\partial w_r} \cdot p_{xx}(x, t). \end{aligned} \quad (18)$$

Once these derivatives are obtained, they can be substituted into Eq. (15) to assemble the full Jacobian matrix J . The LM update is then computed as

$$\Delta W = (J^T J + \kappa I)^{-1} J^T F, \quad (19)$$

where $\kappa > 0$ is the damping parameter controlling the transition between Gauss–Newton and gradient-descent steps [26].

2.2.3. Connection between Jacobian and gradient

In standard PINNs, when the loss function is defined as in Eq. (4) and optimized using quasi-Newton methods such as BFGS or LBFGS, the gradient of the loss function must be evaluated at each iteration.

Let the weights and biases be reshaped and ordered as in Eq. (13). Recall from Eq. (15) that $J_{i,r} = \frac{\partial f_i}{\partial w_r}$, where f_i denotes the residual at the i -th

collocation point and w_r is the r -th component of the parameter vector W . The r -th component of the gradient vector G is then given by

$$\frac{\partial L}{\partial w_r} = \frac{2}{n} \sum_{i=1}^n \frac{\partial f_i}{\partial w_r} f_i = \frac{2}{n} \sum_{i=1}^n J_{i,r} f_i. \quad (20)$$

In matrix form, this expression can be written compactly as

$$G = \frac{2}{n} J^T F. \quad (21)$$

where J denotes the Jacobian matrix and F is the nonlinear system defined in Eq. (6).

This relation highlights that the Jacobian matrix required by LM also naturally appears in the gradient computation used by BFGS and related methods. Consequently, the construction of the Jacobian is not an additional overhead unique to LM, but rather a quantity that is implicitly required in gradient-based optimization. Assuming that the computational cost of evaluating the Jacobian and the gradient is comparable, the main difference in overall computational complexity between LM and BFGS arises from their respective update steps.

2.3. PINNs for the inverse problem

We next consider inverse problems. Since the formulation closely follows that of the forward problem, only the key differences are described.

Consider a general PDE of the form a

$$u_t + \mathcal{N}(u, \lambda) = 0, \quad x \in \Omega, \quad t \in [0, T], \quad (22)$$

with certain initial and boundary conditions, where $\mathcal{N}(\cdot, \lambda)$ denotes a nonlinear differential operator and $\lambda = \{\lambda_1, \lambda_2, \dots\}$ represents a set of unknown parameters. In the inverse problem setting, given partial observations of the solution u and the known structure of the PDE, the objective is to identify λ while simultaneously approximating $u(x, t)$.

The solution is approximated by a neural network $u(x, t, W)$ with trainable weights and biases W . Let $\{(x_i, t_i), u_i^*\}_{i=1}^n$ be a set of collocation points and corresponding observed solution values. Assuming that the initial and boundary conditions are incorporated into the network architecture [38], the weights and biases W and the unknown parameters λ can be learned by minimizing the loss function

$$L(W, \lambda) = \frac{1}{n} \sum_{i=1}^n (f_i(W, \lambda))^2 + \frac{1}{n} \sum_{i=1}^n (g_i(W))^2, \quad (23)$$

where

$$f_i(W, \lambda) = u_t(x_i, t_i, W) + \mathcal{N}(u(x_i, t_i, W), \lambda), \quad i = 1, \dots, n, \quad (24)$$

represents the residual of the PDE, and

$$g_i(W) = u(x_i, t_i, W) - u_i^*, \quad i = 1, \dots, n. \quad (25)$$

quantifies the error between the predicted and observed data or solution. In practice, inverse problems typically involve significantly fewer collocation points than forward problems.

Rather than minimizing Eq. (23) directly, the problem can be formulated as a nonlinear system

$$F(W, \lambda) = \begin{bmatrix} F_1(W, \lambda) \\ F_2(W) \end{bmatrix} = \mathbf{0}, \quad (26)$$

with

$$F_1(W, \lambda) = \begin{bmatrix} f_1(W, \lambda) \\ \vdots \\ f_n(W, \lambda) \end{bmatrix}, \quad F_2(W) = \begin{bmatrix} g_1(W) \\ \vdots \\ g_n(W) \end{bmatrix}. \quad (27)$$

This system can then be solved using LM [24, 25].

In the case of inverse problems, the derivatives of the neural network function with respect to x and t are computed in the same way as in the forward problem. Next, consider the same reordered vector W that contains all weights and biases. Since the inverse problem involves unknown parameters λ , the full set of trainable parameters is given by

$$W = [W_1 \ B_1 \ W_2 \ B_2 \ W_3 \ B_3 \ \lambda]^T. \quad (28)$$

If m denotes the total number of network weights and biases and m_λ the number of unknown PDE parameters, then $W \in \mathbb{R}^{m+m_\lambda}$.

The key distinction between forward and inverse problems lies in the structure of the Jacobian matrix. For n collocation points, the Jacobian $J \in \mathbb{R}^{2n \times (m+m_\lambda)}$ takes the block form

$$J = \begin{bmatrix} J_1 & J_3 \\ J_2 & \mathbf{0} \end{bmatrix}, \quad (29)$$

where

$$J_1 = \begin{bmatrix} \frac{\partial f_1}{\partial w_1} & \dots & \frac{\partial f_1}{\partial w_m} \\ \vdots & \ddots & \vdots \\ \frac{\partial f_n}{\partial w_1} & \dots & \frac{\partial f_n}{\partial w_m} \end{bmatrix}, \quad J_2 = \begin{bmatrix} \frac{\partial g_1}{\partial w_1} & \dots & \frac{\partial g_1}{\partial w_m} \\ \vdots & \ddots & \vdots \\ \frac{\partial g_n}{\partial w_1} & \dots & \frac{\partial g_n}{\partial w_m} \end{bmatrix}, \quad J_3 = \begin{bmatrix} \frac{\partial f_1}{\partial \lambda_1} & \dots & \frac{\partial f_1}{\partial \lambda_{m_\lambda}} \\ \vdots & \ddots & \vdots \\ \frac{\partial f_n}{\partial \lambda_1} & \dots & \frac{\partial f_n}{\partial \lambda_{m_\lambda}} \end{bmatrix}. \quad (30)$$

For $r = 1, \dots, m$, the derivatives with respect to network parameters are given by

$$\begin{aligned}\frac{\partial f_i}{\partial w_r} &= \frac{\partial(u_t(x_i, t_i, W) + \mathcal{N}(u(x_i, t_i, W), \lambda))}{\partial w_r} \\ &= \frac{\partial u_t(x_i, t_i, W)}{\partial w_r} + \mathcal{N}_{w_r}(u(x_i, t_i, W), \lambda),\end{aligned}\tag{31}$$

and,

$$\begin{aligned}\frac{\partial g_i}{\partial w_r} &= \frac{\partial(u(x_i, t_i, W) - u_i^*)}{\partial w_r} \\ &= \frac{\partial u(x_i, t_i, W)}{\partial w_r}.\end{aligned}\tag{32}$$

For the unknown PDE parameters λ_r , $r = 1, \dots, m_\lambda$, we have

$$\begin{aligned}\frac{\partial f_i}{\partial \lambda_r} &= \frac{\partial(u_t(x_i, t_i, W) + \mathcal{N}(u(x_i, t_i, W), \lambda))}{\partial \lambda_r} \\ &= \mathcal{N}_{\lambda_r}(u(x_i, t_i, W)).\end{aligned}\tag{33}$$

As an illustration, if

$$\mathcal{N}(u) = \lambda_1 u u_x + \lambda_2 u_{xx},\tag{34}$$

then

$$\mathcal{N}_{\lambda_1}(u) = u u_x, \quad \mathcal{N}_{\lambda_2}(u) = u_{xx}.\tag{35}$$

The required derivatives of u , u_t , u_x , and u_{xx} with respect to w_r can be computed using the same differentiation techniques described in the forward problem.

Furthermore, the gradient of the loss function (23) can be expressed in terms of the Jacobian. For $r = 1, \dots, m$,

$$\frac{\partial L}{\partial w_r} = \frac{2}{n} \sum_{i=1}^n \frac{\partial f_i}{\partial w_r} f_i + \frac{2}{n} \sum_{i=1}^n \frac{\partial g_i}{\partial w_r} g_i.\tag{36}$$

and for $r = 1, \dots, m_\lambda$,

$$\frac{\partial L}{\partial \lambda_r} = \frac{2}{n} \sum_{i=1}^n \frac{\partial f_i}{\partial \lambda_r} f_i.\tag{37}$$

In compact form,

$$G = \begin{bmatrix} \frac{2}{n} J_1^T F_1 + \frac{2}{n} J_2^T F_2 \\ \frac{2}{n} J_3^T F_1 \end{bmatrix}.\tag{38}$$

3. Experimental results

For experimental purposes, we compare the performance of LM and BFGS algorithms for training PINNs. For BFGS, the gradient is computed using the Jacobian–gradient relationships derived in the previous section. To ensure a fair comparison, differences in computational cost per iteration are taken into account. Since each LM iteration requires solving a linear system and is therefore more computationally demanding than a single BFGS iteration, the maximum number of iterations is set to 4000 for LM and 20000 for BFGS. This choice aims to balance the overall computational effort and allows both methods to achieve comparable optimization progress.

For LM, we employ MATLAB’s built-in `fsolve` function, which is designed for solving nonlinear systems of equations. For BFGS, we use MATLAB’s `fminunc` function, a general-purpose unconstrained optimizer that supports quasi-Newton methods. It is worth noting that LM naturally targets nonlinear systems, whereas BFGS is formulated for the minimization of scalar-valued objective functions. To enable a consistent comparison, after each LM iteration we evaluate the corresponding loss function using Eq. (4) for forward problems and Eq. (23) for inverse problems. This allows the convergence behavior of both methods to be assessed using the same loss-based metric.

In all experiments, the hyperbolic tangent (`tanh`) activation function is used, as it is standard in PINNs. Moreover, the same set of collocation points is employed for both optimization methods to ensure that any observed performance differences are attributable solely to the optimization algorithm rather than to variations in the training data.

All simulations are conducted on a computer equipped with an Intel Core i5-10400 CPU with six cores. Although this hardware is not tailored for high-performance computing, it reflects a practical and commonly accessible computational environment for PINNs research without dedicated GPU resources. For reproducibility, all experiments are performed using MATLAB R2024a or R2024b.

3.1. Forward problem: Burgers equation

We begin with the forward problem for the one-dimensional Burgers equation, as originally considered in Raissi et al. [1],

$$\begin{aligned} u_t + uu_x - \frac{0.01}{\pi}u_{xx} &= 0, \quad x \in [-1, 1], \quad t \in [0, 1], \\ u(x, 0) &= -\sin(\pi x), \\ u(-1, t) &= u(1, t) = 0. \end{aligned} \tag{39}$$

To enforce the initial and boundary conditions, we construct the trial solution

$$u = \tilde{u}(1 - x^2)t - \sin(\pi x). \quad (40)$$

which automatically satisfies all prescribed conditions. For training, we sample $n = 10000$ collocation points from the spatiotemporal domain $[-1, 1] \times [0, 1]$. We begin with the shallow architecture $\text{NN}(2, 25, 25, 1)$, which contains a total of 751 trainable weights and biases.

Fig. 2a shows the full spatiotemporal solution obtained using LM. In Fig. 2b, we compare the solutions produced by LM and BFGS at $t = 0.25$, 0.50, and 0.75 with the reference solution reported in [41]. The corresponding absolute errors are shown in Fig. 2c, where LM achieves errors approximately three orders of magnitude smaller than those obtained by BFGS.

The evolution of the loss function during training is shown in Fig. 2d. Due to different iteration limits, the BFGS loss is reported every five iterations up to 20000 iterations, whereas the LM loss is reported at every iteration up to 4000 iterations. At convergence, LM achieves a final loss value of 8.1×10^{-8} , which is significantly smaller than the 1.4×10^{-3} obtained by BFGS. Moreover, the total computational time for LM is 2281 seconds, compared to 4442 seconds for BFGS, indicating that LM attains substantially higher accuracy with roughly half the computational cost.

To further quantify accuracy, we compute the relative L_2 error against the reference solution evaluated on a uniform grid of 1001×1001 points, with $\Delta x = 2 \times 10^{-3}$ and $\Delta t = 10^{-3}$. The resulting relative L_2 errors are 2.0×10^{-4} for LM and 2.2×10^{-2} for BFGS, confirming the superior accuracy of LM for this problem.

For comparison, the original PINNs paper [1] employed a much deeper architecture consisting of eight hidden layers with 20 neurons each (3021 trainable parameters) and used LBFGS for optimization. Despite the substantially deeper network, the reported relative L_2 error was 6.7×10^{-4} . In contrast, our shallow network with only two hidden layers achieves a lower error of 2.0×10^{-4} when trained using LM, while using approximately four times fewer trainable parameters. This result reinforces that network depth and size alone do not determine the accuracy of PINNs when an appropriate optimization strategy is employed.

Finally, Tab. 2 summarizes the loss values, relative L_2 errors, and computational times for several network sizes trained using LM. As expected, increasing the number of neurons improves accuracy. Notably, even $\text{NN}(2, 15, 15, 1)$ achieves reasonable accuracy, suggesting that moderately sized shallow networks offer an effective balance between efficiency and precision.

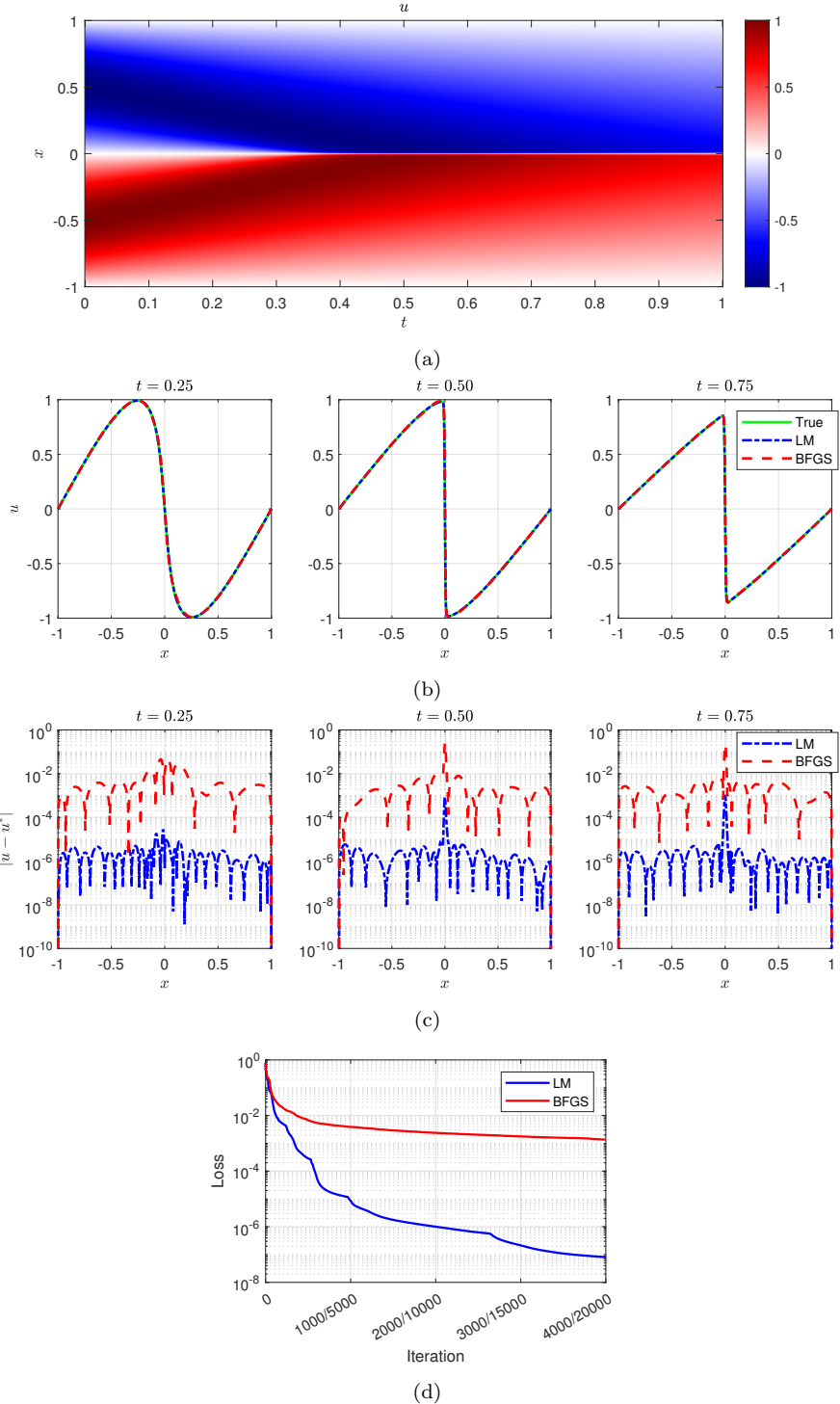


Figure 2: (a) Neural network solution of the Burgers equation obtained using LM. (b) Solutions computed by LM and BFGS at selected time slices. (c) Absolute errors corresponding to the LM and BFGS solutions. (d) Training loss histories of LM and BFGS.

Table 2: Comparison of loss values, relative L_2 errors, and computational times for different network sizes obtained using LM for the Burgers equation.

Network	Loss	Relative L_2 error	Time
NN(2, 5, 5, 1)	$2.2 \cdot 10^{-2}$	$5.3 \cdot 10^{-2}$	116
NN(2, 10, 10, 1)	$1.0 \cdot 10^{-3}$	$2.4 \cdot 10^{-2}$	312
NN(2, 15, 15, 1)	$1.6 \cdot 10^{-5}$	$2.3 \cdot 10^{-3}$	850
NN(2, 20, 20, 1)	$1.2 \cdot 10^{-6}$	$5.4 \cdot 10^{-4}$	1561
NN(2, 25, 25, 1)	$8.1 \cdot 10^{-8}$	$2.0 \cdot 10^{-4}$	2281

3.2. Forward problem: nonlinear Schrödinger equation

We next consider a more challenging example, the nonlinear Schrödinger equation similar to the one used in the original PINNs paper [1]

$$\begin{aligned}
 &iu_t + \frac{1}{2}u_{xx} + |u|^2 u = 0, \quad x \in [-5, 5], \quad t \in [0, \pi/2], \\
 &u(x, 0) = 2 \operatorname{sech}(x) \cos^2\left(\frac{\pi}{10}x\right), \\
 &u(-5, t) = u(5, t), \\
 &u_x(-5, t) = u_x(5, t).
 \end{aligned} \tag{41}$$

where u is complex-valued.

We decompose u into its real and imaginary parts,

$$u(x, t) = v(x, t) + iw(x, t), \tag{42}$$

which yields the real-valued system

$$\begin{aligned}
 &-w_t + \frac{1}{2}v_{xx} + (v^2 + w^2)v = 0, \\
 &v_t + \frac{1}{2}w_{xx} + (v^2 + w^2)w = 0.
 \end{aligned} \tag{43}$$

Unlike [1], which employs a single PINN with two outputs, we use two separate PINNs to approximate \tilde{v} and \tilde{w} , trained simultaneously. To enforce the initial conditions, we define

$$v = \tilde{v}t + 2 \operatorname{sech}(x) \cos^2\left(\frac{\pi}{10}x\right), \quad w = \tilde{w}t. \tag{44}$$

Periodic boundary conditions are enforced by mapping the spatial coordinate x to $\sin(2\pi x/P)$ and $\cos(2\pi x/P)$ with $P = 10$ [38]. Thus, the network input is defined as

$$X = [\sin(2\pi x/P) \ \cos(2\pi x/P) \ t]. \tag{45}$$

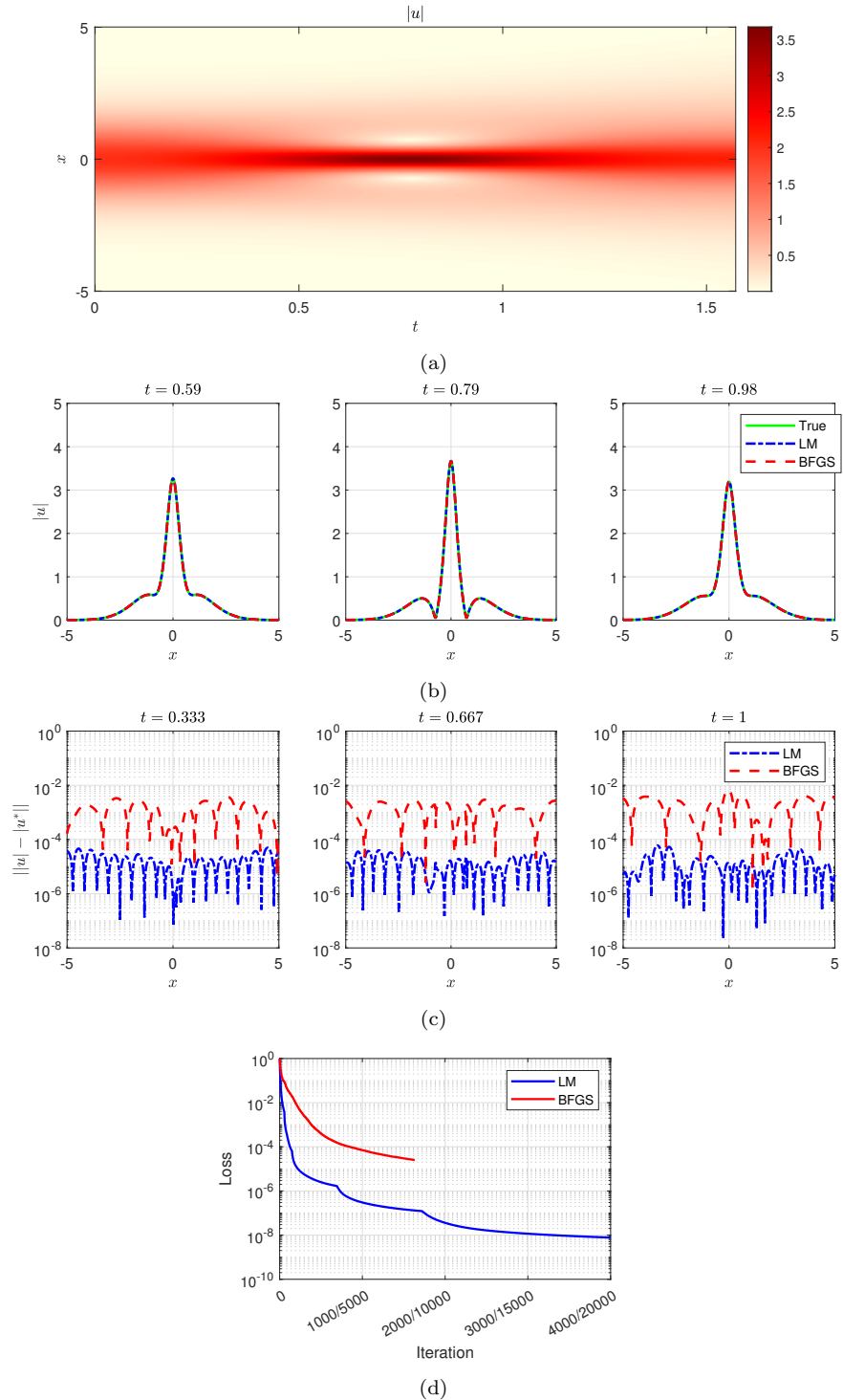


Figure 3: (a) Neural network solution of the nonlinear Schrödinger equation obtained using LM. (b) Solutions computed by LM and BFGS at selected time slices. (c) Absolute errors corresponding to the LM and BFGS solutions. (d) Training loss histories of LM and BFGS.

Table 3: Comparison of loss values, relative L_2 errors, and computational times for different network sizes obtained using LM for the nonlinear Schrödinger equation.

Network	Loss	Relative L_2 error	Time
$2 \times \text{NN}(3, 5, 5, 1)$	$8.5 \cdot 10^{-3}$	$9.1 \cdot 10^{-2}$	447
$2 \times \text{NN}(3, 10, 10, 1)$	$6.6 \cdot 10^{-5}$	$3.4 \cdot 10^{-3}$	1307
$2 \times \text{NN}(3, 15, 15, 1)$	$4.3 \cdot 10^{-7}$	$2.4 \cdot 10^{-4}$	3856
$2 \times \text{NN}(3, 20, 20, 1)$	$2.4 \cdot 10^{-8}$	$4.3 \cdot 10^{-5}$	5875
$2 \times \text{NN}(3, 25, 25, 1)$	$7.7 \cdot 10^{-9}$	$2.1 \cdot 10^{-5}$	10303

We again use $n = 10000$ collocation points and begin with two $\text{NN}(3, 25, 25, 1)$ networks, one for v and one for w , resulting in 1552 total trainable parameters.

Figs. 3a and 3b present the spatiotemporal solution and time-slice comparisons at $t = 0.59, 0.79$, and 0.98 . The reference solution is computed using a fourth-order Runge–Kutta method with time step $\Delta t = (\pi/2) \times 10^{-6}$ and Fourier spectral discretization in space with $\Delta x = 10/2^9$. Absolute errors are shown in Fig. 3c, where LM achieves errors approximately two orders of magnitude smaller than those obtained by BFGS.

Fig. 3d shows the training loss histories. BFGS stagnates after 8164 iterations with a final loss of 2.5×10^{-5} , whereas LM reaches a much smaller loss of 7.7×10^{-9} within 4000 iterations. The computational time for LM is 10303 seconds, compared to 5825 seconds for BFGS at early termination. Extrapolating BFGS to 20000 iterations yields an estimated time of approximately 14270 seconds.

Relative L_2 errors are computed on a grid of 2^9 spatial points and 1001 temporal points, giving 2.1×10^{-5} for LM and 2.7×10^{-3} for BFGS. These results further confirm the superior performance of LM.

For comparison, Raissi et al. [1] also solved a similar nonlinear Schrödinger equation using a considerably larger neural network with four hidden layers of 100 neurons each, amounting to 40902 trainable parameters, and reported a relative L_2 error of 1.97×10^{-3} . In contrast, our method employs two shallow PINNs with only two hidden layers, totaling 1552 parameters, yet attains a markedly lower relative L_2 error of 2.1×10^{-5} . This represents an improvement of nearly two orders of magnitude in accuracy while requiring more than 25 times fewer parameters, demonstrating the efficiency of shallow PINNs when coupled with an effective optimization strategy.

Finally, Tab. 3 reports results for different network sizes trained using LM. Even $\text{NN}(3, 10, 10, 1)$ and $\text{NN}(3, 15, 15, 1)$ provide reasonable accuracy, indicating that shallow architectures can be highly effective for this problem.

3.3. Inverse problem: Allen–Cahn equation

Next, we consider the application of PINNs to inverse problems. As the first example, we study the Allen–Cahn equation [1] given by

$$\begin{aligned} u_t - 0.0001u_{xx} + 5u^3 - 5u &= 0, \quad x \in [-1, 1], \quad t \in [0, 1], \\ u(x, 0) &= x^2 \cos(\pi x), \\ u(-1, t) &= u(1, t) = -1. \end{aligned} \tag{46}$$

For the inverse problem, we consider the generalized form

$$u_t + \lambda_1 u_{xx} + \lambda_2 u^3 + \lambda_3 u = 0 \tag{47}$$

where λ_1 , λ_2 , and λ_3 are treated as unknown parameters to be identified simultaneously with the solution u .

To enforce the initial and boundary conditions, we construct the neural network approximation as

$$u = \tilde{u}(1 - x^2)t + x^2 \cos(\pi x). \tag{48}$$

For training, we randomly select $n = 2000$ collocation points within the space-time domain. The reference solution values at these points are obtained via time integration using the fourth-order Runge–Kutta method with a time step of $\Delta t = 10^{-6}$. Spatial derivatives are approximated using the central finite difference with $\Delta x = 2 \times 10^{-4}$. After solving the equation over the interval $t \in [0, 1]$, we sample the solution on a uniform grid of 1001×1001 points in space and time, with $\Delta x = 2 \times 10^{-3}$ and $\Delta t = 10^{-3}$. The true parameters are set to $\lambda_1 = -0.0001$, $\lambda_2 = 5$, and $\lambda_3 = -5$. Parameter identification is performed using the network architecture $\text{NN}(2, 25, 25, 1)$, resulting in a total of 754 trainable parameters, including the network weights, biases, and the unknown parameters λ_1 , λ_2 , and λ_3 .

The full neural network solution obtained using LM is shown in Fig. 4a. In Fig. 4b, we compare the solutions obtained by LM and BFGS at $t = 0.25$, 0.50 , and 0.75 against the reference solution computed using the fourth-order Runge–Kutta method. The corresponding absolute errors are presented in Fig. 4c.

Fig. 4d displays the training loss histories for both optimization algorithms. LM attains a final loss value of 1.2×10^{-8} , which is significantly lower than the 1.7×10^{-5} achieved by BFGS. However, LM requires approximately 2110 seconds of computational time, which is about 2.5 times longer than that required by BFGS (approximately 877 seconds).

Fig. 4e illustrates the evolution of the estimated parameters λ_1 , λ_2 , and λ_3 during the early stages of training. Despite requiring fewer iterations, LM

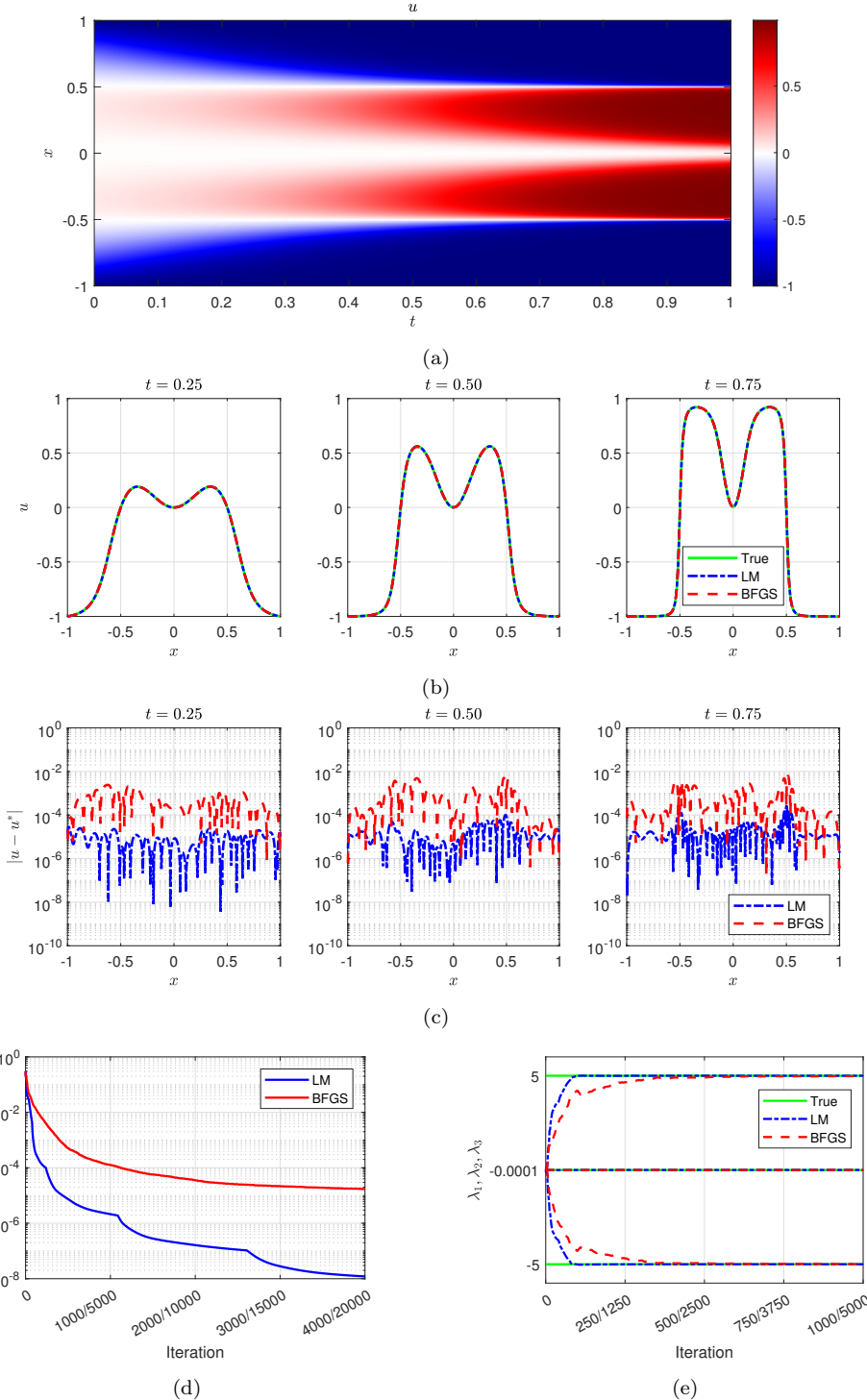


Figure 4: (a) Neural network solution of the Allen–Cahn equation obtained using LM. (b) Solutions computed by LM and BFGS at selected time slices. (c) Absolute errors corresponding to the LM and BFGS solutions. (d) Training loss histories of LM and BFGS. (e) Evolution of the estimated parameters during training for LM and BFGS.

Table 4: Identified PDEs obtained using LM and BFGS for the Allen–Cahn equation.

Method	PDE
True	$u_t - 0.00010000u_{xx} + 5.00000u^3 - 5.00000u$
LM	$u_t - 0.00010003u_{xx} + 4.99983u^3 - 4.99994u$
BFGS	$u_t - 0.000144231u_{xx} + 5.00372u^3 - 5.00402u$

Table 5: Comparison of loss values, absolute percentage errors (APEs), and computational times obtained using LM and BFGS for the Allen–Cahn equation.

Method	Loss	APE λ_1	APE λ_2	APE λ_3	Time
LM	$1.2 \cdot 10^{-8}$	0.0027	0.0034	0.0011	2110
BFGS	$1.7 \cdot 10^{-5}$	44.2306	0.0744	0.0804	877

converges to the true parameter values both faster and more accurately than BFGS.

A quantitative comparison of the identified parameters obtained by LM and BFGS is summarized in Tab. 4, with the corresponding absolute percentage errors (APEs) reported in Tab. 5. As shown, LM consistently outperforms BFGS in identifying all parameters. Overall, these results demonstrate the effectiveness of shallow PINNs trained with LM for high-fidelity parameter identification in nonlinear PDEs.

Finally, Tab. 6 compares the loss values, APEs, and computational times for different network architectures trained using LM. Increasing the number of neurons generally improves both loss values and parameter accuracy. Notably, even the smaller network $\text{NN}(2, 15, 15, 1)$ yields reasonably accurate results, with APEs for all parameters remaining below 1%. This configuration also outperforms BFGS (see Tab. 5) in terms of both accuracy and computational time.

Table 6: Comparison of loss values, absolute percentage errors (APEs), and computational times for different network sizes obtained using LM for the Allen–Cahn equation.

Network	Loss	APE λ_1	APE λ_2	APE λ_3	Time
$\text{NN}(2, 5, 5, 1)$	$1.5 \cdot 10^{-2}$	1618.1627	25.4738	22.5804	42
$\text{NN}(2, 10, 10, 1)$	$5.7 \cdot 10^{-4}$	72.1185	2.6754	2.2376	113
$\text{NN}(2, 15, 15, 1)$	$8.8 \cdot 10^{-7}$	0.3691	0.0033	0.0036	262
$\text{NN}(2, 20, 20, 1)$	$8.1 \cdot 10^{-8}$	0.6517	0.0082	0.0016	836
$\text{NN}(2, 25, 25, 1)$	$1.2 \cdot 10^{-8}$	0.0027	0.0034	0.0011	2110

3.4. Inverse problem: three-dimensional Bratu equation

As the final example, we consider a time-independent inverse problem governed by the three-dimensional Bratu equation. While the previous examples involved a single spatial variable, this case demonstrates that shallow PINNs can also be effectively applied to problems with higher spatial dimensionality. The three-dimensional Bratu equation is given by [37]

$$\begin{aligned}\Delta u + Ce^u &= 0, \quad (x, y, z) \in \Omega \\ u(x, y, z) &= 0, \quad (x, y, z) \in \partial\Omega\end{aligned}\tag{49}$$

where $\Omega = [0, 1]^3$ and $\Delta u = u_{xx} + u_{yy} + u_{zz}$. For the inverse problem, we consider

$$\Delta u + \lambda_1 e^{\lambda_2 u} = 0\tag{50}$$

with λ_1 and λ_2 treated as unknown parameters to be identified along with the solution u .

To enforce the boundary conditions, the neural network approximation is constructed as

$$u = \tilde{u}(x - x^2)(y - y^2)(z - z^2).\tag{51}$$

For training, we randomly select $n = 2000$ collocation points within the domain. The corresponding reference solution is obtained using the symmetric finite difference method (SFDM) [37] with 300 uniform subintervals (301 grid points) in each spatial direction. The true parameters are set to $\lambda_1 = C = 2$ and $\lambda_2 = 1$. The identification is performed using the architecture NN(3, 25, 25, 1), resulting in a total of 778 trainable parameters, including the network weights, biases, and the unknown parameters λ_1 and λ_2 .

The neural network solution obtained using LM is shown in Fig. 5a, where the slice $z = 0.5$ is fixed for visualization purposes. In Fig. 5b, we compare the solutions obtained by LM and BFGS at $z = 0.5$ and $y = 0.25, 0.50$, and 0.75 against the reference solution computed using SFDM. The corresponding absolute errors are presented in Fig. 5c.

Fig. 5d presents the training loss curves for both optimization algorithms. LM achieves a final loss value of 5.7×10^{-10} , which is substantially lower than the 3.8×10^{-5} obtained by BFGS. In terms of computational cost, LM requires approximately 2470 seconds, which is slightly higher than the 1851 seconds required by BFGS.

Fig. 5e shows the evolution of the estimated parameters λ_1 and λ_2 during the early stages of training. Despite using fewer iterations, LM converges to the true parameter values more rapidly and accurately than BFGS.

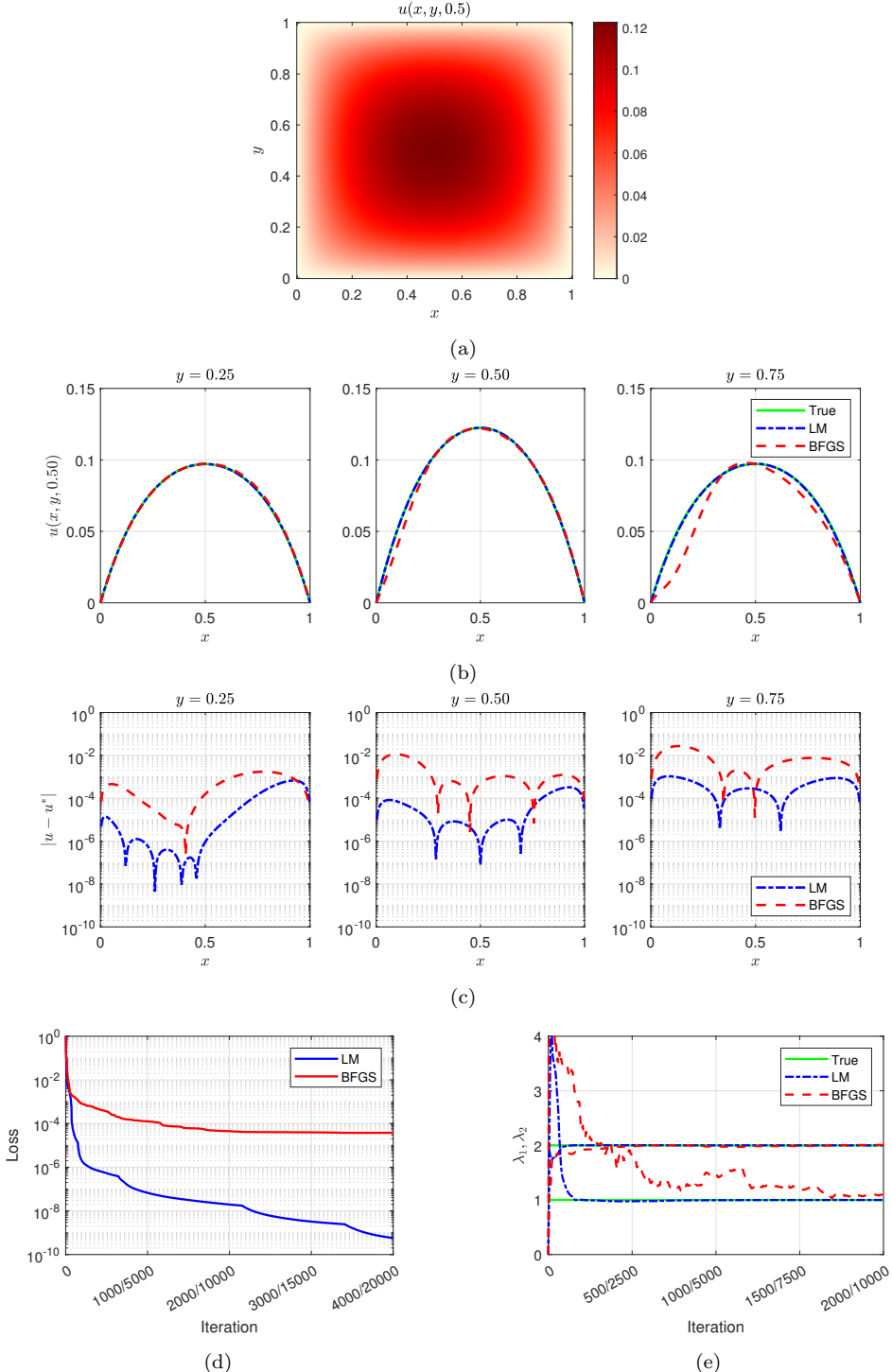


Figure 5: (a) Neural network solution of the three-dimensional Bratu equation obtained using LM. (b) Solutions computed by LM and BFGS at selected time slices. (c) Absolute errors corresponding to the LM and BFGS solutions. (d) Training loss histories of LM and BFGS. (e) Evolution of the estimated parameters during training for LM and BFGS.

Table 7: Identified PDEs obtained using LM and BFGS for the three-dimensional Bratu equation.

Method	PDE
True	$\Delta u + 2.00000e^{1.00000u}$
LM	$\Delta u + 1.99994e^{1.00018u}$
BFGS	$\Delta u + 2.01510e^{0.97944u}$

Table 8: Comparison of loss values, absolute percentage errors (APEs), and computational times obtained using LM and BFGS for the three-dimensional Bratu equation.

Method	Loss	APE λ_1	APE λ_2	Time
LM	$5.7 \cdot 10^{-10}$	0.0028	0.0180	2470
BFGS	$3.8 \cdot 10^{-5}$	0.7549	2.0562	1851

A quantitative comparison of the identified parameters is summarized in Tab. 7, with the corresponding APEs reported in Tab. 8. As indicated in the tables, LM consistently outperforms BFGS in identifying both parameters. These results further highlight the effectiveness of shallow PINNs trained with LM for parameter identification in nonlinear PDEs.

Finally, Tab. 9 compares the loss values, APEs, and computational times for various network architectures trained using LM. Increasing the number of neurons generally improves both accuracy and loss values. Notably, even the smaller network NN(3, 10, 10, 1) yields reasonably accurate results, with APEs for all parameters remaining below 1%, and also outperforms BFGS (see Tab. 8) in terms of both accuracy and computational time.

4. Conclusion

In this work, we propose solving PDEs using shallow PINNs by reformulating the underlying problems as nonlinear systems. These systems are then

Table 9: Comparison of loss values, absolute percentage errors (APEs), and computational times for different network sizes obtained using LM for the three-dimensional Bratu equation.

Network	Loss	APE λ_1	APE λ_2	Time
NN(3, 5, 5, 1)	$1.4 \cdot 10^{-4}$	2.0648	77.2285	87
NN(3, 10, 10, 1)	$1.2 \cdot 10^{-7}$	0.0169	0.7576	211
NN(3, 15, 15, 1)	$1.4 \cdot 10^{-7}$	0.0213	0.0337	404
NN(3, 20, 20, 1)	$2.4 \cdot 10^{-8}$	0.0090	0.1370	1051
NN(3, 25, 25, 1)	$5.7 \cdot 10^{-10}$	0.0028	0.0180	2470

solved using the Levenberg–Marquardt (LM) algorithm, a second-order optimization method well known for its robustness and efficiency in nonlinear systems or least-squares problems.

We derive exact analytical expressions for the derivatives of neural networks with respect to their input variables. These derivations play a central role in constructing an accurate PINNs framework (see Fig. 1), as they explicitly reveal the connections between the network output and its spatial and temporal derivatives. In particular, they clarify how the network weights and biases are shared across the solution and derivative branches, ensuring consistency and computational efficiency, and they provide a transparent illustration of how initial and boundary conditions are enforced.

Based on these analytical expressions, we present explicit formulas for computing the Jacobian matrix required by LM. We further demonstrate that, within the PINNs framework, the Jacobian computation is intrinsically related to the gradient computation used in first-order and quasi-Newton methods such as BFGS. This relationship is established for both forward and inverse problem formulations.

Numerical experiments are conducted for both forward and inverse problems involving the Burgers, Schrödinger, Allen–Cahn, and three-dimensional Bratu equations. Using a fixed architecture $\text{NN}(a, 25, 25, 1)$ in all cases, LM consistently outperforms BFGS. Specifically, LM achieves final loss values on the order of 10^{-8} to 10^{-10} , corresponding to improvements of three to five orders of magnitude over BFGS. Moreover, LM reaches this accuracy with substantially fewer iterations (4000 versus 20000). In forward problems, LM also produces relative L_2 errors that are approximately two orders of magnitude smaller, indicating a more accurate approximation of the PDE solutions. In inverse problems, LM not only yields lower loss values but also converges more rapidly and accurately to the true parameter values, highlighting its effectiveness for parameter identification.

In some cases, we also compare our results with those reported in the original PINNs literature [1] and show that our approach attains higher accuracy, despite employing significantly shallower and smaller network architectures. These results indicate that network depth alone does not determine accuracy in PINNs, and that shallow networks can attain high accuracy when trained using appropriate optimization strategies.

Despite the use of standard CPU-based hardware and the absence of GPU acceleration, the proposed shallow PINNs trained with LM exhibit rapid convergence and high accuracy, demonstrating their computational efficiency and practical applicability. This highlights the feasibility of the proposed approach for researchers with limited computational resources.

Overall, our results indicate that a wide class of PDEs can be efficiently

solved using shallow PINNs when the problem is reformulated as a nonlinear system and solved with LM. For practical applications, we recommend starting with shallow architectures such as $\text{NN}(a, 10, 10, 1)$ or $\text{NN}(a, 15, 15, 1)$, which offer a favorable balance between accuracy and computational cost, and increasing the number of neurons only when the problem exhibits complex features such as sharp gradients or multiscale behavior.

Beyond its computational advantages, this work also has educational value. By explicitly deriving the analytical structure of PINNs, including the computation of derivatives, the construction of Jacobians, and their relationship to gradient-based methods, this study provides deeper insight into the internal mechanisms of PINNs. The derived formulas are directly transferable to other optimization strategies and can facilitate the implementation of PINNs beyond standard automatic differentiation pipelines.

Future studies could explore the applicability of shallow PINNs trained with LM for solving PDEs in higher spatial dimensions. While we also present results in three spatial dimensions that demonstrate the efficiency and accuracy of this approach, it remains unclear whether these performance advantages persist as the dimensionality increases, particularly in light of the associated growth in computational complexity and memory requirements. The curse of dimensionality may introduce additional challenges, such as the need for more training data or more expressive network architectures, even when employing shallow networks.

In addition, further research is needed to improve the integration of LM-based training with automatic differentiation frameworks. At present, most LM solvers do not natively support automatic differentiation, limiting their direct use within deep learning libraries such as TensorFlow or PyTorch. Developing efficient, differentiable LM solvers would significantly enhance the accessibility and scalability of this approach. In this context, incorporating improved LM formulations that avoid explicit storage and manipulation of large Jacobian matrices, such as those proposed in [27], represents a promising direction for reducing memory usage and accelerating training in large-scale PINNs.

Acknowledgement

HS acknowledges support by Khalifa University through the Research & Innovation Grants under project IDs KU-INT-RIG-2023-8474000617 and KU-INT-RIG-2024-8474000789.

Declaration of generative AI and AI-assisted technologies in the writing process

During the preparation of this work, the authors used ChatGPT to improve the language and readability. After using this tool, the authors reviewed and edited the content as needed and take full responsibility for the content of the publication.

References

- [1] M. Raissi, P. Perdikaris, G. E. Karniadakis, Physics-informed neural networks: A deep learning framework for solving forward and inverse problems involving nonlinear partial differential equations, *Journal of Computational physics* 378 (2019) 686–707.
- [2] J. Han, A. Jentzen, W. E, Solving high-dimensional partial differential equations using deep learning, *Proceedings of the National Academy of Sciences* 115 (34) (2018) 8505–8510.
- [3] E. R. Putri, M. L. Shahab, M. Iqbal, I. Mukhlash, A. Hakam, L. Mardianto, H. Susanto, A deep-genetic algorithm (deep-GA) approach for high-dimensional nonlinear parabolic partial differential equations, *Computers & Mathematics with Applications* 154 (2024) 120–127.
- [4] L. Lu, P. Jin, G. Pang, Z. Zhang, G. E. Karniadakis, Learning nonlinear operators via DeepONet based on the universal approximation theorem of operators, *Nature Machine Intelligence* 3 (3) (2021) 218–229.
- [5] Z. Li, N. Kovachki, K. Azizzadenesheli, B. Liu, K. Bhattacharya, A. Stuart, A. Anandkumar, Fourier neural operator for parametric partial differential equations, *arXiv preprint arXiv:2010.08895* (2020).
- [6] H. Lee, I. S. Kang, Neural algorithm for solving differential equations, *Journal of Computational Physics* 91 (1) (1990) 110–131.
- [7] M. Dissanayake, N. Phan-Thien, Neural-network-based approximations for solving partial differential equations, *Communications in Numerical Methods in Engineering* 10 (3) (1994) 195–201.
- [8] I. E. Lagaris, A. Likas, D. I. Fotiadis, Artificial neural networks for solving ordinary and partial differential equations, *IEEE Transactions on Neural Networks* 9 (5) (1998) 987–1000.

- [9] I. E. Lagaris, A. C. Likas, D. G. Papageorgiou, Neural-network methods for boundary value problems with irregular boundaries, *IEEE Transactions on Neural Networks* 11 (5) (2000) 1041–1049.
- [10] D. P. Kingma, J. Ba, Adam: A method for stochastic optimization, arXiv preprint arXiv:1412.6980 (2014).
- [11] D. C. Liu, J. Nocedal, On the limited memory BFGS method for large scale optimization, *Mathematical Programming* 45 (1) (1989) 503–528.
- [12] E. Kiyani, K. Shukla, J. F. Urbán, J. Darbon, G. E. Karniadakis, Optimizing the optimizer for physics-informed neural networks and kolmogorov-arnold networks, *Computer Methods in Applied Mechanics and Engineering* 446 (2025) 118308.
- [13] S. Cuomo, V. S. Di Cola, F. Giampaolo, G. Rozza, M. Raissi, F. Piccialli, Scientific machine learning through physics-informed neural networks: Where we are and what's next, *Journal of Scientific Computing* 92 (3) (2022) 88.
- [14] W.-F. Hu, Y.-J. Shih, T.-S. Lin, M.-C. Lai, A shallow physics-informed neural network for solving partial differential equations on static and evolving surfaces, *Computer Methods in Applied Mechanics and Engineering* 418 (2024) 116486.
- [15] G.-B. Huang, D. H. Wang, Y. Lan, Extreme learning machines: a survey, *International Journal of Machine Learning and Cybernetics* 2 (2011) 107–122.
- [16] G. Fabiani, E. Galaris, L. Russo, C. Siettos, Parsimonious physics-informed random projection neural networks for initial value problems of odes and index-1 daes, *Chaos: An Interdisciplinary Journal of Nonlinear Science* 33 (4) (2023).
- [17] E. Schiassi, R. Furfaro, C. Leake, M. De Florio, H. Johnston, D. Mortari, Extreme theory of functional connections: A fast physics-informed neural network method for solving ordinary and partial differential equations, *Neurocomputing* 457 (2021) 334–356.
- [18] V. Dwivedi, B. Srinivasan, Physics informed extreme learning machine (PIELM)—a rapid method for the numerical solution of partial differential equations, *Neurocomputing* 391 (2020) 96–118.

- [19] A. A. Ramabathiran, P. Ramachandran, SPINN: sparse, physics-based, and partially interpretable neural networks for PDEs, *Journal of Computational Physics* 445 (2021) 110600.
- [20] P. Shi, Z. Zeng, T. Liang, Physics-informed ConvNet: Learning physical field from a shallow neural network, *Communications in Nonlinear Science and Numerical Simulation* 132 (2024) 107911.
- [21] J. Rishi, A. Gafoor, S. Kumar, D. Subramani, On the training efficiency of shallow architectures for physics informed neural networks, in: *International Conference on Computational Science*, Springer, 2024, pp. 363–377.
- [22] F. Calabro, G. Fabiani, C. Siettos, Extreme learning machine collocation for the numerical solution of elliptic PDEs with sharp gradients, *Computer Methods in Applied Mechanics and Engineering* 387 (2021) 114188.
- [23] G. Fabiani, F. Calabro, L. Russo, C. Siettos, Numerical solution and bifurcation analysis of nonlinear partial differential equations with extreme learning machines, *Journal of Scientific Computing* 89 (2) (2021) 44.
- [24] K. Levenberg, A method for the solution of certain non-linear problems in least squares, *Quarterly of Applied Mathematics* 2 (2) (1944) 164–168.
- [25] D. W. Marquardt, An algorithm for least-squares estimation of nonlinear parameters, *Journal of the Society for Industrial and Applied Mathematics* 11 (2) (1963) 431–441.
- [26] M. T. Hagan, M. B. Menhaj, Training feedforward networks with the Marquardt algorithm, *IEEE Transactions on Neural Networks* 5 (6) (1994) 989–993.
- [27] B. M. Wilamowski, H. Yu, Improved computation for Levenberg-Marquardt training, *IEEE Transactions on Neural Networks* 21 (6) (2010) 930–937.
- [28] J. de Jesús Rubio, Stability analysis of the modified Levenberg-Marquardt algorithm for the artificial neural network training, *IEEE Transactions on Neural Networks and Learning Systems* 32 (8) (2020) 3510–3524.

- [29] X. Fu, S. Li, M. Fairbank, D. C. Wunsch, E. Alonso, Training recurrent neural networks with the Levenberg-Marquardt algorithm for optimal control of a grid-connected converter, *IEEE Transactions on Neural Networks and Learning Systems* 26 (9) (2014) 1900–1912.
- [30] C. Lv, Y. Xing, J. Zhang, X. Na, Y. Li, T. Liu, D. Cao, F.-Y. Wang, Levenberg-Marquardt backpropagation training of multilayer neural networks for state estimation of a safety-critical cyber-physical system, *IEEE Transactions on Industrial Informatics* 14 (8) (2017) 3436–3446.
- [31] H. Calandra, S. Gratton, E. Riccietti, X. Vasseur, On a multilevel Levenberg-Marquardt method for the training of artificial neural networks and its application to the solution of partial differential equations, *Optimization Methods and Software* 37 (1) (2022) 361–386.
- [32] G. K. Yadav, B. Srinivasan, Shallow physics informed neural networks using Levenberg-Marquardt optimization, in: OPT2020: 12th Annual Workshop on Optimization for Machine Learning, 2020.
- [33] M. L. Shahab, H. Susanto, Neural networks for bifurcation and linear stability analysis of steady states in partial differential equations, *Applied Mathematics and Computation* 483 (2024) 128985.
- [34] M. L. Shahab, H. Susanto, Corrigendum to "Neural networks for bifurcation and linear stability analysis of steady states in partial differential equations" [Appl. Math. Comput. 483 (2024) 128985], *Applied Mathematics and Computation* 495 (2025) 129319.
- [35] M. L. Shahab, F. A. Suheri, R. Kusdiantara, H. Susanto, Physics-informed neural networks for high-dimensional solutions and snaking bifurcations in nonlinear lattices, *Physica D: Nonlinear Phenomena* (2025) 134836.
- [36] J. Taylor, W. Wang, B. Bala, T. Bednarz, Optimizing the optimizer for data driven deep neural networks and physics informed neural networks, arXiv preprint arXiv:2205.07430 (2022).
- [37] M. L. Shahab, H. Susanto, H. Hatzikirou, A finite difference method with symmetry properties for the high-dimensional Bratu equation, *Applied Mathematics and Computation* 489 (2025) 129136.
- [38] L. Lu, R. Pestourie, W. Yao, Z. Wang, F. Verdugo, S. G. Johnson, Physics-informed neural networks with hard constraints for inverse design, *SIAM Journal on Scientific Computing* 43 (6) (2021) B1105–B1132.

- [39] A. G. Baydin, B. A. Pearlmutter, A. A. Radul, J. M. Siskind, Automatic differentiation in machine learning: A survey, *Journal of Machine Learning Research* 18 (2018) 1–43.
- [40] M. Abadi, P. Barham, J. Chen, Z. Chen, A. Davis, J. Dean, M. Devin, S. Ghemawat, G. Irving, M. Isard, et al., TensorFlow: a system for large-scale machine learning, in: 12th USENIX Symposium on Operating Systems Design and Implementation (OSDI 16), 2016, pp. 265–283.
- [41] C. Basdevant, M. Deville, P. Haldenwang, J. Lacroix, J. Ouazzani, R. Peyret, P. Orlandi, A. Patera, Spectral and finite difference solutions of the Burgers equation, *Computers & Fluids* 14 (1) (1986) 23–41.

Appendix A. Derivatives with respect to weights and biases

In this section, we provide the formulas for computing $\frac{\partial \tilde{u}}{\partial w_r}$, $\frac{\partial \tilde{u}_t}{\partial w_r}$, $\frac{\partial \tilde{u}_x}{\partial w_r}$, and $\frac{\partial \tilde{u}_{xx}}{\partial w_r}$. To simplify and accelerate the computations, we adopt the vectorized form $X = [\mathbf{x} \; \mathbf{t}]$, as described in Section 2.2.1. We begin with the weights and biases closest to the output layer. The derivatives with respect to the bias B_3 are given by

$$\begin{aligned} \frac{\partial \tilde{u}}{\partial B_3} &= \mathbf{1} \\ \frac{\partial \tilde{u}_t}{\partial B_3} &= \mathbf{0} \\ \frac{\partial \tilde{u}_x}{\partial B_3} &= \mathbf{0} \\ \frac{\partial \tilde{u}_{xx}}{\partial B_3} &= \mathbf{0}. \end{aligned} \tag{A.1}$$

The derivatives with respect to the weights $w_j \in W_3$, for $j = 1, \dots, m_2$, are given by

$$\begin{aligned} \frac{\partial \tilde{u}}{\partial w_j} &= H_2(:, j) \\ \frac{\partial \tilde{u}_t}{\partial w_j} &= H_{2,t}(:, j) \\ \frac{\partial \tilde{u}_x}{\partial w_j} &= H_{2,x}(:, j) \\ \frac{\partial \tilde{u}_{xx}}{\partial w_j} &= H_{2,xx}(:, j). \end{aligned} \tag{A.2}$$

In this case, we use the notation $(:, j)$ to represent all rows in the j -th column of a matrix. This is a common convention in MATLAB. We adopt this notation because many of the matrices already include indices.

The derivatives with respect to the biases $b_k \in B_2$, for $k = 1, \dots, m_2$, are given by

$$\begin{aligned} \frac{\partial \tilde{u}}{\partial b_k} &= \sigma'(h_2(:, k)) \cdot W_3(k) \\ \frac{\partial \tilde{u}_t}{\partial b_k} &= \sigma''(h_2(:, k)) \cdot h_{2,t}(:, k) \cdot W_3(k) \\ \frac{\partial \tilde{u}_x}{\partial b_k} &= \sigma''(h_2(:, k)) \cdot h_{2,x}(:, k) \cdot W_3(k) \\ \frac{\partial \tilde{u}_{xx}}{\partial b_k} &= \sigma'''(h_2(:, k)) \cdot h_{2,x}^2(:, k) \cdot W_3(k) \\ &\quad + \sigma''(h_2(:, k)) \cdot h_{2,xx}(:, k) \cdot W_3(k). \end{aligned} \tag{A.3}$$

Similar to Section 2.2.1, the dot operator \cdot here denotes element-wise multiplication.

The derivatives with respect to the weights $w_{j,k} \in W_2$, for $j = 1, \dots, m_1$ and $k = 1, \dots, m_2$, are given by

$$\begin{aligned} \frac{\partial \tilde{u}}{\partial w_{j,k}} &= H_1(:, j) \cdot \sigma'(h_2(:, k)) \cdot W_3(k) \\ \frac{\partial \tilde{u}_t}{\partial w_{j,k}} &= H_1(:, j) \cdot \sigma''(h_2(:, k)) \cdot h_{2,t}(:, k) \cdot W_3(k) \\ &\quad + H_{1,t}(:, j) \cdot \sigma'(h_2(:, k)) \cdot W_3(k) \\ \frac{\partial \tilde{u}_x}{\partial w_{j,k}} &= H_1(:, j) \cdot \sigma''(h_2(:, k)) \cdot h_{2,x}(:, k) \cdot W_3(k) \\ &\quad + H_{1,x}(:, j) \cdot \sigma'(h_2(:, k)) \cdot W_3(k) \\ \frac{\partial \tilde{u}_{xx}}{\partial w_{j,k}} &= H_1(:, j) \cdot \sigma'''(h_2(:, k)) \cdot h_{2,x}^2(:, k) \cdot W_3(k) \\ &\quad + 2H_{1,x}(:, j) \cdot \sigma''(h_2(:, k)) \cdot h_{2,x}(:, k) \cdot W_3(k) \\ &\quad + H_1(:, j) \cdot \sigma''(h_2(:, k)) \cdot h_{2,xx}(:, k) \cdot W_3(k) \\ &\quad + H_{1,xx}(:, j) \cdot \sigma'(h_2(:, k)) \cdot W_3(k). \end{aligned} \tag{A.4}$$

The derivatives with respect to the biases $b_k \in B_1$, for $k = 1, \dots, m_1$, are

given by

$$\begin{aligned}
\frac{\partial \tilde{u}}{\partial b_k} &= \sigma'(h_1(:, k)) \cdot ((\sigma'(h_2) \cdot W_3^T) W_2(k, :)^T) \\
\frac{\partial \tilde{u}_t}{\partial b_k} &= \sigma'(h_1(:, k)) \cdot ((\sigma''(h_2) \cdot h_{2,t} \cdot W_3^T) W_2(k, :)^T) \\
&\quad + \sigma''(h_1(:, k)) \cdot h_{1,t}(:, k) \cdot ((\sigma'(h_2) \cdot W_3^T) W_2(k, :)^T) \\
\frac{\partial \tilde{u}_x}{\partial b_k} &= \sigma'(h_1(:, k)) \cdot ((\sigma''(h_2) \cdot h_{2,x} \cdot W_3^T) W_2(k, :)^T) \\
&\quad + \sigma''(h_1(:, k)) \cdot h_{1,x}(:, k) \cdot ((\sigma'(h_2) \cdot W_3^T) W_2(k, :)^T) \\
\frac{\partial \tilde{u}_{xx}}{\partial b_k} &= \sigma'(h_1(:, k)) \cdot ((\sigma'''(h_2) \cdot h_{2,xx}^2 \cdot W_3^T) W_2(k, :)^T) \\
&\quad + \sigma''(h_1(:, k)) \cdot h_{1,x}(:, k) \cdot ((2\sigma''(h_2) \cdot h_{2,x} \cdot W_3^T) W_2(k, :)^T) \\
&\quad + \sigma'(h_1(:, k)) \cdot ((\sigma''(h_2) \cdot h_{2,xx} \cdot W_3^T) W_2(k, :)^T) \\
&\quad + \sigma'''(h_1(:, k)) \cdot h_{1,x}^2(:, k) \cdot ((\sigma'(h_2) \cdot W_3^T) W_2(k, :)^T) \\
&\quad + \sigma''(h_1(:, k)) \cdot h_{1,xx}(:, k) \cdot ((\sigma'(h_2) \cdot W_3^T) W_2(k, :)^T).
\end{aligned} \tag{A.5}$$

Finally, the derivatives with respect to the weights $w_{j,k} \in W_1$, for $j = 1, \dots, m_1$ and $k = 1, \dots, m_2$, are given by

$$\begin{aligned}
\frac{\partial \tilde{u}}{\partial w_{j,k}} &= X(:,j) \cdot \sigma'(h_1(:,k)) \cdot ((\sigma'(h_2) \cdot W_3^T) W_2(k,:)^T) \\
\frac{\partial \tilde{u}_t}{\partial w_{j,k}} &= X(:,j) \cdot \sigma'(h_1(:,k)) \cdot ((\sigma''(h_2) \cdot h_{2,t} \cdot W_3^T) W_2(k,:)^T) \\
&\quad + X(:,j) \cdot \sigma''(h_1(:,k)) \cdot h_{1,t}(:,k) \cdot ((\sigma'(h_2) \cdot W_3^T) W_2(k,:)^T) \\
&\quad + X_t(:,j) \cdot \sigma'(h_1(:,k)) \cdot ((\sigma'(h_2) \cdot W_3^T) W_2(k,:)^T) \\
\frac{\partial \tilde{u}_x}{\partial w_{j,k}} &= X(:,j) \cdot \sigma'(h_1(:,k)) \cdot ((\sigma''(h_2) \cdot h_{2,x} \cdot W_3^T) W_2(k,:)^T) \\
&\quad + X(:,j) \cdot \sigma''(h_1(:,k)) \cdot h_{1,x}(:,k) \cdot ((\sigma'(h_2) \cdot W_3^T) W_2(k,:)^T) \\
&\quad + X_x(:,j) \cdot \sigma'(h_1(:,k)) \cdot ((\sigma'(h_2) \cdot W_3^T) W_2(k,:)^T) \\
\frac{\partial \tilde{u}_{xx}}{\partial w_{j,k}} &= X(:,j) \cdot \sigma'(h_1(:,k)) \cdot ((\sigma'''(h_2) \cdot h_{2,x}^2 \cdot W_3^T) W_2(k,:)^T) \\
&\quad + X(:,j) \cdot \sigma''(h_1(:,k)) \cdot h_{1,x}(:,k) \cdot ((2\sigma''(h_2) \cdot h_{2,x} \cdot W_3^T) W_2(k,:)^T) \\
&\quad + X_x(:,j) \cdot \sigma'(h_1(:,k)) \cdot ((2\sigma''(h_2) \cdot h_{2,x} \cdot W_3^T) W_2(k,:)^T) \\
&\quad + X(:,j) \cdot \sigma'(h_1(:,k)) \cdot ((\sigma''(h_2) \cdot h_{2,xx} \cdot W_3^T) W_2(k,:)^T) \\
&\quad + X(:,j) \cdot \sigma'''(h_1(:,k)) \cdot h_{1,x}^2(:,k) \cdot ((\sigma'(h_2) \cdot W_3^T) W_2(k,:)^T) \\
&\quad + X_x(:,j) \cdot \sigma''(h_1(:,k)) \cdot 2h_{1,x}(:,k) \cdot ((\sigma'(h_2) \cdot W_3^T) W_2(k,:)^T) \\
&\quad + X(:,j) \cdot \sigma''(h_1(:,k)) \cdot h_{1,xx}(:,k) \cdot ((\sigma'(h_2) \cdot W_3^T) W_2(k,:)^T) \\
&\quad + X_{xx}(:,j) \cdot \sigma'(h_1(:,k)) \cdot ((\sigma'(h_2) \cdot W_3^T) W_2(k,:)^T).
\end{aligned} \tag{A.6}$$